Supporting Information

Photochemical transformation of graphene oxide in sunlight

Wen-Che Hou[*,†,⊥], *Indranil Chowdhury*[†], *David G. Goodwin Jr.*[‡], *Matthew Henderson*[§], *Howard Fairbrother*[‡], *Dermont Bouchard*[§], *Richard G. Zepp*[*,§]

[†]*National Research Council Associate, National Exposure Research Laboratory, Ecosystems Research Division, U. S. Environmental Protection Agency, Athens, GA, 30605*

[⊥]*Department of Environmental Engineering, National Cheng Kung University, Tainan City, Taiwan, 70101*

[‡]*Department of Chemistry, Johns Hopkins University, Baltimore, MD 21218*

[§]*National Exposure Research Laboratory, Ecosystems Research Division, U. S. Environmental Protection Agency, Athens, GA, 30605*

**Address correspondence to either author. Phone: +886 62757575 ext.65842 (W. C. H.). (706) 355-8117, Fax: +886 6 2752790 (W. C. H.), (706) 355-8007 (R. G. Z.), E-mail: whou@mail.ncku.edu.tw (W. C. H.); Richard.Zepp@epa.gov (R. G. Z.).*

Manuscript prepared for publication in: Environmental Science & Technology

Pages: 13

Figures: S1-6

Table: S1

Procedure for dissolved oxygen level studies

We examined the effect of dissolved oxygen (DO) level on GO's photoreactivity under air-equilibrated and O_2-deficient conditions. To create O_2-deficient samples, we removed dissolved O_2 from GO samples by bubbling pure N_2 gas into the tubes for 1 h prior to irradiation. N_2 bubbling was performed by penetrating a needle through the septa and below the liquid surface; another needle above the liquid surface equated pressure in the tubes with the atmosphere above the septa.

Method for Measuring CO_2 evolved from GO during photolysis

To measure CO_2 that evolved during irradiation, atmospheric CO_2 was removed by bubbling solutions with CO_2-free air or CO_2-free N_2 as described above to examine the effect of DO. While gas-bubbling with CO_2-free air or CO_2-free N_2 lowered the inorganic carbon (IC) level, it was still detectable in the dark control samples, although the concentration was significantly smaller than in irradiated samples. To measure the CO_2 produced, a 3-mL aliquot of headspace from the quartz tube was analyzed using gas chromatography (GC). The total inorganic carbon species concentration was calculated, accounting for gaseous CO_2 in the headspace, dissolved CO_2, bicarbonate, and carbonate; pH values were measured in samples not intended for CO_2 analysis.

CO_2 measurements were performed on an Agilent 6890 gas chromatograph (GC) equipped with a thermal-conductivity detector (TCD). Headspace samples were separated using a Hayesep DB packed column (30 m × 0.125 mm × 80/100 mesh; Supelco Analytical, St. Louis, MO) with helium maintained at a constant flow of 30 mL/min as the carrier gas. The inlet temperature was 105 ^oC and the initial oven temperature of 70 ^oC was held for 8 min, then ramped to 150 ^oC at 80 ^oC/min and held for an additional 7 min.

Procedure for photoproduct preparation

Separate experiments to prepare sufficient GO photoproducts for characterizations used large volumes (0.7 L) of 40 mg/L GO samples that were irradiated in a similar manner as described earlier for various time periods under air- or N_2-equilibrated condition. After irradiation, samples were

vacuum-concentrated and freeze-dried.

Characterizations of GO photoproducts

Mass spectrometry: This procedure was used to determine the low molecular-weight products formed during GO photolysis. Aqueous GO samples before and after light irradiation were passed through 0.2 μm filters. The filtrates were collected and diluted 1:1 (v/v) with acetonitrile and fortified with 0.1% formic acid before direct infusion into a Thermo Quantum Ultra mass spectrometer equipped with an ESI source (Thermo Fisher Scientific). Full scan mass spectra were acquired over the range of 50 to 1200 m/z in positive ion mode for 5 min. The spray voltage was maintained at 3.5 kV, capillary temperature was 275 °C and the sheath and auxiliary gas pressures were 30 and 15 arbitrary units, respectively. Following full scan acquisition, neutral loss scans were acquired over the range of 50-500 m/z to investigate the loss of 17, 18, and 28 m/z using a collision pressure of 1.5 mTorr and collision energy of -20 eV.

UV-Visible absorbance: A Perkin Elmer Lambda 35 UV-visible absorbance spectrophotometer equipped with a 1-cm light path quartz cuvette was used to follow the progress of GO photoreactions. Dissolved organic carbon (DOC): DOC concentrations were quantitated by a Shimadzu TOC-VCPH carbon analyzer.

Fluorescence: We used a Horiba Fluorolog 3-221 spectrofluorometer with a 1-cm light path quartz cuvette to characterize photoluminescence (PL) of GO samples before and after irradiation. Scans were corrected for the instruments configuration and converted into quinine sulfate equivalents. We post-processed data to remove the Raman and Raleigh scattering peaks with an in-house Fluorescence Toolbox (version 2.0).[1] The reported fluorescent intensity was corrected for the inner filter effect using the method described by Gauthier et al.[2] Since the PL intensity reported in the study is corrected for screening of excitation and emission light by the sample absorbance values, the values are reflective of the intrinsic PL of samples.

Raman: A Renishaw inVia Raman spectrophotometer equipped with 532-nm laser recorded the

Raman spectra. Samples for Raman spectroscopy were prepared by air-drying a few drops of GO samples on copper foils.

X-ray Photoelectron Spectroscopy (XPS): For XPS analysis, approximately 3 mg of each GO irradiated sample was dusted onto copper tape (0.5×0.5 cm^2) until it was completely covered. Samples were loaded into a PHI 5600 XPS system ($P_{base} < 5 \times 10^{-9}$ Torr) and analyzed using Mg Kα X-rays (1253.6 eV, 15 kV, 300 W) and a high energy electron energy analyzer operating at a constant pass-energy of 58.7 eV with a scan rate of 0.125 eV/step (50 ms/step). XP spectra were processed by commercially available software (CasaXPS). The concentrations of oxygen-containing functional groups were determined from each sample by peak-fitting the C (1s) region, taking advantage of clearly discernible peaks due to GO's large oxygen-to-carbon ratio. For component-fitting of the C(1s) region, each spectrum was given a Shirley background and energy-adjusted to the CC/CH fitted spectral feature within the C (1s) region at 284.5 eV. Spectra of the dark control and irradiated samples were fitted with CC/CH, C-O, C=O, and O-C=O features. The CC/CH peak position was set at 284.5 eV and FWHM determined by fitting the C (1s) region of the most photo-reduced GO samples which had the most intense CC/CH component (see Figure 3). Based on reports in the literature, the C-O peak was determined to be 286.8 eV and the FWHM determined by analyzing native GO samples where C-O species are the dominant feature (see Figure 3). The C=O (287.7 eV) and O-C=O (289.1 eV) features were determined from average peak positions used in the literature for GO,[3–7] and within a ± 0.2 eV range of the C=O and O-C=O values used in reference polymers from Briggs et al. (polyvinyl methyl ketone (PVMK) at 287.97 eV and polymethyl methacrylate (PMMA) at 289.03 eV, respectively).[8] Peak positions and FWHM values for all components were allowed to drift no more than ± 0.2 eV of the peak position for all samples analyzed.

Attenuated total reflectance infrared spectroscopy (ATR-IR): ATR-IR monitored changes in distribution of oxygen functional groups on GO following irradiation. All spectra were acquired using a Thermo Scientific Nicolet iS5 ATR-IR with a diamond crystal and a dTGS room-temperature detector

(< 0.8 cm^{-1} resolution). Five hundred scans were taken for each IR spectrum obtained.

Dynamic Light Scattering (DLS): The hydrodynamic diameter and zeta potential were determined by a DLS particle sizer (Malvern Zetasizer Nano-ZS).

Atomic Force Microscopy (AFM): Physical dimensions of photo-transformed GO were determined from images taken by a Veeco Multimode AFM with a Nanoscope V controller and an E scanner (Bruker AXC Inc., Madison, WI). Samples for AFM imaging were prepared on positively-charged poly-*L*-lysine hydrobromide-coated Si wafers. Images were taken under ScanAsyst-Air mode with a Silicon Nitride cantilever (ScanAsyst-Air, Bruker AXC Inc., Madison, WI). AFM images were further analyzed for distribution of thickness, diameter and surface area using Nanoscope Analysis software (Bruker AXC Inc., Madison, WI).

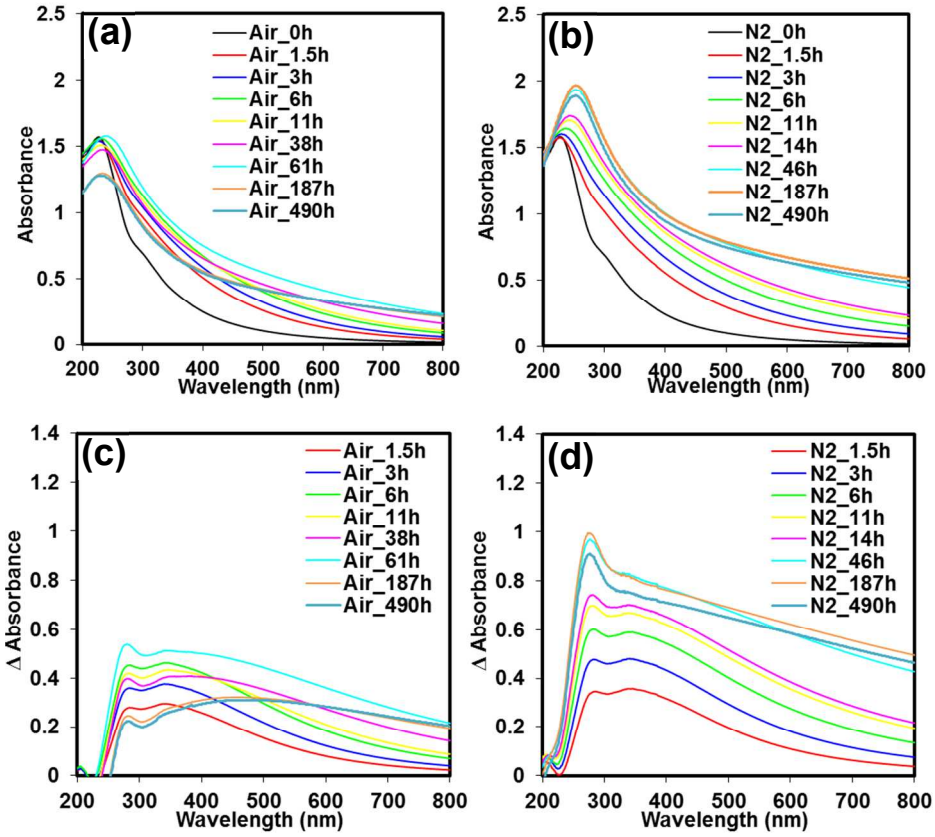

Figure S1. UV-visible absorbance spectra of GO before and after sunlight irradiation, showing time-dependent changes in absorbance of (a) air-equilibrated samples and (b) N_2-saturated samples, as well as the corresponding difference in spectra of (c) air-equilibrated samples and (d) N_2-saturated samples. The difference spectra presented in (c) and (d) are obtained by subtracting absorbance value of the dark control sample (parent GO) from absorbance values of samples exposed to sunlight.

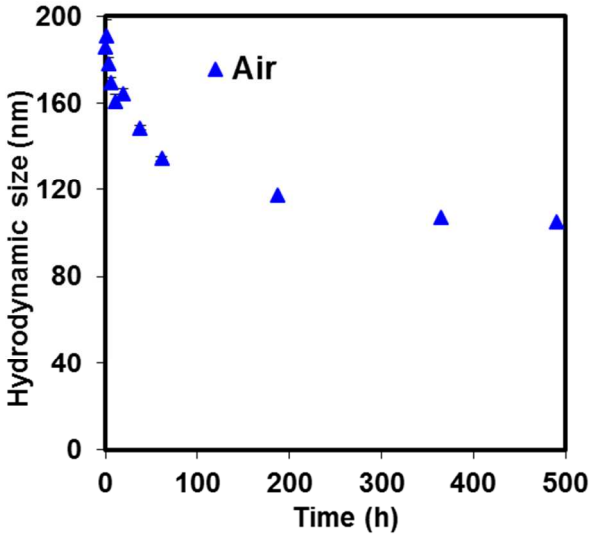

Figure S2. Hydrodynamic size evolution of air-equilibrated samples under simulated sunlight exposure.

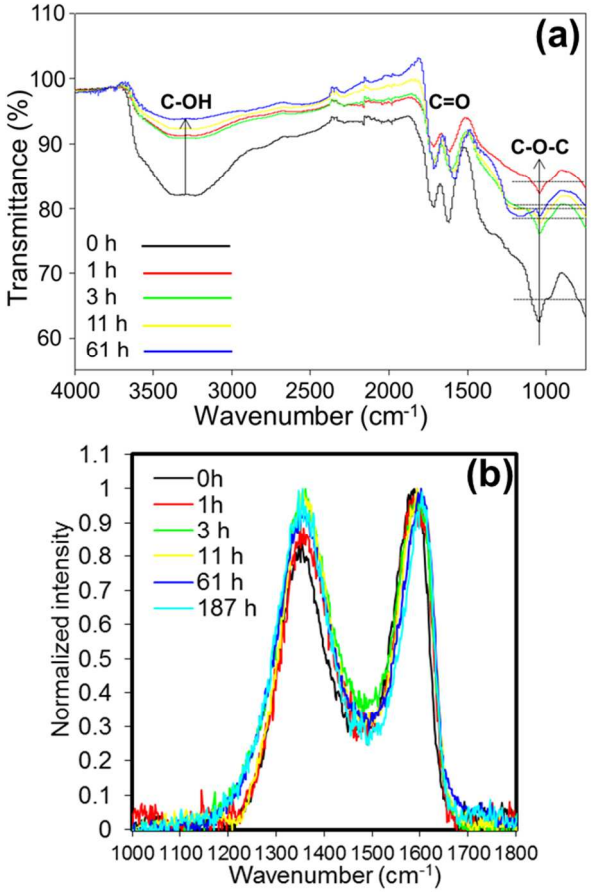

120

121 **Figure S3.** Spectral changes of air-saturated GO samples with sunlight exposure, showing (a) ATR-IR

122 spectra, and (b) Raman spectra of photo-transformed GO products.

123

124

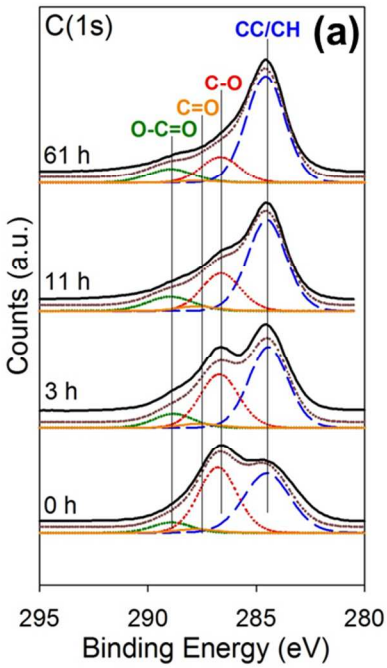

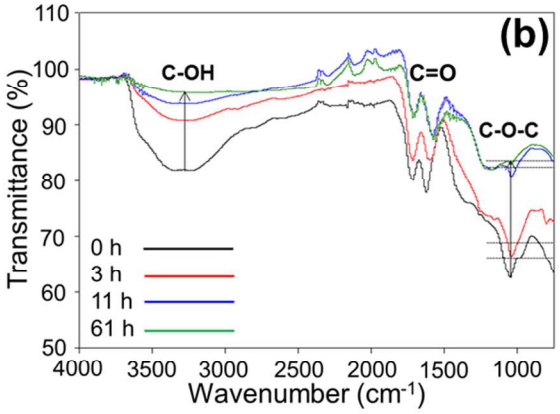

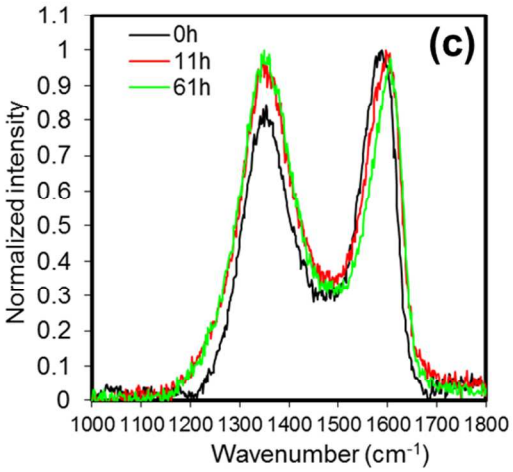

Sample	O:C	%CC/CH	%C-O	%C=O	%O-C=O
0 h	0.58	46	43	2	7
3 h	0.56	53	35	3	9
11 h	0.50	60	25	3	11
61 h	0.40	70	17	1	11

Figure S4. Spectral changes of N_2-saturated GO samples with sunlight exposure, showing (a) XPS spectra, (b) ATR-IR spectra, and (c) Raman spectra of photo-transformed GO products. The table shows changes in the oxygen-to-carbon ratio and functional groups of GO samples during irradiation.

N_2-saturated GO samples also lost significant oxygen-containing groups, decreasing from ~52% to ~29% for total % O after 61 h of irradiation, compared to the decrease from ~52% to ~34% in air-equilibrated samples after irradiation for the same period. XPS, ATR-IR, and Raman spectra (Figure S4a-c) collectively show GO photoproducts formed in N_2-saturated samples are similar to those in air-equilibrated samples (Figure 4 and Figure S3).

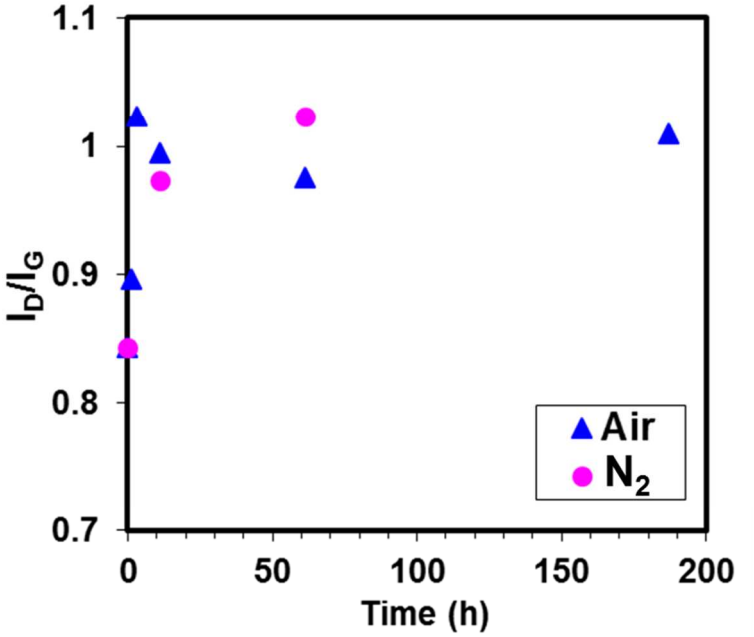

Figure S5. I_D/I_G ratio of GO samples as a function of irradiation time.

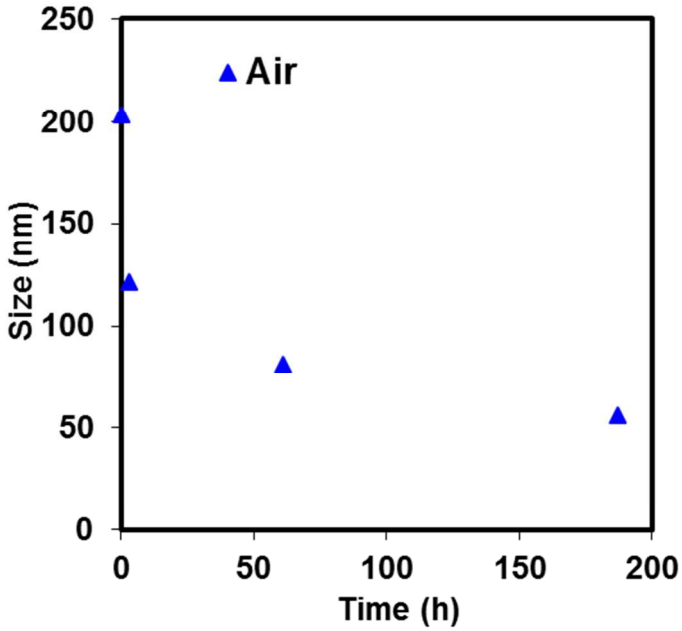

Figure S6. Size changes revealed by AFM images of samples before and after light irradiation. The data shown here are from the images reported in Figure 1d-g.

Table S1. Summary of the kinetics for changes in functional groups of GO samples irradiated under sunlight.

Functionality	**condition**	k_{obs} **(h^{-1})**	R^2
C-O	Air	0.0097 ± 0.0108	0.73
	N_2	0.0128 ± 0.0184	0.82
CC/CH	Air	0.0039 ± 0.0056	0.62
	N_2	0.0054 ± 0.0085	0.79
C=O	Air	0.0058 ± 0.0086	0.22
	N_2	0.0133 ± 0.0182	0.83
O-C=O	Air	0.0068 ± 0.007	0.76
	N_2	0.0046 ± 0.0194	0.34

References

(1) Zepp, R. G.; Sheldon, W. M.; Moran, M. A. Dissolved organic fluorophores in southeastern US coastal waters: correction method for eliminating Rayleigh and Raman scattering peaks in excitation–emission matrices. *Marine Chemistry* **2004**, *89*, 15–36.

(2) Gauthier, T. D.; Shane, E. C.; Guerin, W. F.; Seitz, W. R.; Grant, C. L. Fluorescence quenching method for determining equilibrium constants for polycyclic aromatic hydrocarbons binding to dissolved humic materials. *Environ. Sci. Technol.* **1986**, *20*, 1162–1166.

(3) Matsumoto, Y.; Koinuma, M.; Ida, S.; Hayami, S.; Taniguchi, T.; Hatakeyama, K.; Tateishi, H.; Watanabe, Y.; Amano, S. Photoreaction of Graphene Oxide Nanosheets in Water. *J. Phys. Chem. C*.

(4) Matsumoto, Y.; Koinuma, M.; Kim, S. Y.; Watanabe, Y.; Taniguchi, T.; Hatakeyama, K.; Tateishi, H.; Ida, S. Simple Photoreduction of Graphene Oxide Nanosheet under Mild Conditions. *ACS Appl. Mater. Interfaces* **2010**, *2*, 3461–3466.

(5) Chandra, V.; Park, J.; Chun, Y.; Lee, J. W.; Hwang, I.-C.; Kim, K. S. Water-Dispersible Magnetite-Reduced Graphene Oxide Composites for Arsenic Removal. *ACS Nano* **2010**, *4*, 3979–3986.

(6) Guardia, L.; Villar-Rodil, S.; Paredes, J. I.; Rozada, R.; Martínez-Alonso, A.; Tascón, J. M. D. UV light exposure of aqueous graphene oxide suspensions to promote their direct reduction, formation of graphene–metal nanoparticle hybrids and dye degradation. *Carbon* **2012**, *50*, 1014–1024.

(7) Huang, H.; Xia, Y.; Tao, X.; Du, J.; Fang, J.; Gan, Y.; Zhang, W. Highly efficient electrolytic exfoliation of graphite into graphene sheets based on Li ions intercalation–expansion–microexplosion mechanism. *J. Mater. Chem.* **2012**, *22*, 10452–10456.

(8) Briggs, D.; Beamson, G. Primary and secondary oxygen-induced C1s binding energy shifts in x-ray photoelectron spectroscopy of polymers. *Anal. Chem.* **1992**, *64*, 1729–1736.